Saturn's Curiously Corrugated C Ring

M.M. Hedman[1,*], J.A. Burns[1,2], M.W. Evans[1], M.S.Tiscareno[1], C.C.Porco[3]

April 21, 2011

[1] Department of Astronomy, Cornell University, Ithaca NY 14853

[2] Department of Mechanical Engineering, Cornell University, Ithaca NY 14853

[3] CICLOPS-SSI, Boulder CO 80301

[*] To whom correspondence should be addressed, e-mail mmhedman@astro.cornell.edu

ABSTRACT: *In August 2009 the Sun illuminated Saturn's rings from almost exactly edge-on, revealing a subtle corrugation that extends across the entire C ring. This corrugation's amplitude is 2-20 m and its wavelength is 30-80 km. Radial trends in the corrugation's wavelength indicate that this structure –like a similar corrugation previously identified in the D ring– results from differential nodal regression within a ring that became tilted relative to Saturn's equator plane in 1983. We suggest that this initial tilt arose because interplanetary debris struck the rings. The corrugation's radial extent implies that the impacting material was a dispersed cloud of debris instead of a single object, and the corrugation's amplitude indicates that the debris' total mass was* $\sim 10^{11}$-10^{13} *kg.*

The Cassini spacecraft obtained numerous images of Saturn's rings within a few months of Saturn's equinox in August 2009, when the Sun illuminated the rings from almost exactly edge-on. Many of these observations were designed to investigate ring features that would be highlighted by this unusual lighting geometry, such as shadows cast by embedded moonlets or inclined ringlets. Among the most surprising structures revealed by these images was a series of regularly spaced bright and dark bands extending throughout the entire C ring (Fig. 1). Because this periodic banding was not seen in earlier Cassini images, it cannot be ascribed to simple variations in the ring's density or optical depth. Instead, these bands appear to be caused by a vertical corrugation extending across the entire C ring. Broad-scale corrugations have previously been identified in Saturn's D ring [1] and Jupiter's main ring [2]; both these structures appear to have formed within the last few decades when the relevant ring suddenly became tilted relative to its planet's equatorial plane [1, 3]. The C-ring corrugation seems to have been similarly generated, and indeed it was probably created by the same ring-tilting event that produced the D-ring's corrugation.

The amplitudes and wavelengths of the C-ring's periodic brightness variations have been measured using Fourier analyses of selected images (see SOM text 1). The amplitudes of the observed brightness variations change with viewing and illumination geometries as expected for a vertically corrugated ring (see SOM text 2). The corrugation amplitudes derived from a simple photometric model range between 2 and 20 m throughout the C ring (Fig. 2a; SOM text 2 describes systematic uncertainties associated with these estimates), and are thus well below the few-hundred-meter amplitudes of the previously identified D-ring corrugations [1]. Meanwhile, the corrugation wavenumber systematically decreases with increasing distance from Saturn throughout the entire C ring (Fig. 2b), suggesting that the observed corrugations are part of a single coherent structure. Extrapolating the observed trends interior to the C ring, the predicted wavenumber is close to the expected wavenumber of the previously-observed, larger-amplitude D-ring corrugation. The latter has been interpreted as the result of differential nodal regression of an initially inclined ring [1], which suggests that the C-ring corrugations could have been produced by the same process (Fig. 3). Indeed, the radial trends seen in Fig. 2b are consistent with such a model.

A corrugation produced by differential nodal regression of an initially inclined ring should have a radial wavenumber given by (see [1] and SOM text 3)

$$k_z = \left| \frac{\partial \dot{\Omega}}{\partial r} \right| \delta t, \tag{1}$$

where δt is the time that has elapsed since the ring was an inclined sheet, and $\dot{\Omega}(r)$ is the local nodal regression rate. To first order, $\dot{\Omega}$ is determined by Saturn's quadrupole gravitational harmonic J_2 [4, 5], so Eq. 1 can be approximated as:

$$k_z \simeq \frac{21}{4} J_2 \sqrt{\frac{GM_s}{r^5}} \left(\frac{R_s}{r} \right)^2 \delta t, \tag{2}$$

where G is the gravitational constant, M_s is Saturn's mass, r is the ring radius and R_s is the assumed Saturn radius used to normalize J_2. Thus a corrugation produced by differential nodal regression should have $k_z \sim r^{-9/2}$. Including contributions from all Saturn's measured higher-order gravity harmonics [6] yields the solid curves in Figs. 2b and c, which differ slightly from the trend calculated above and match the observed data to within 3%.

The largest deviations from this model include a quasi-periodic wavenumber modulation in the middle C ring and a cluster of low wavenumber values in the outermost C ring ($r > 90{,}000$ km, Fig. 2c). These residuals are correlated with the optical depth structure of the ring (compare Figs. 2c and 2e), and can be ascribed to the C-ring's finite surface mass density σ. The ring's gravity

modifies the local nodal regression rates, producing perturbations to the corrugation wavenumber:

$$\frac{\delta k_z}{k_z} = \frac{\pi G}{2\nu}\left(-\frac{\partial\sigma}{\partial r} + \frac{3\sigma}{r}\right)\delta t, \tag{3}$$

where ν is the vertical epicyclic frequency (see SOM text 3). If we assume the ring's optical depth τ is proportional to its surface mass density σ, then the largest negative residuals in the corrugation wavenumber should occur where the optical depth has the most positive slope and vice versa, as observed. Furthermore, the magnitude of the measured residuals would require that the middle C-ring has σ ~3-6 g/cm^2 (see SOM text 4), consistent with previous estimates [7, 8].

If we only consider regions where the predicted $\delta k_z/k_z$ caused by the ring's self-gravity is less than 0.2% (Fig. 2d and SOM text 5), the wavelength estimates are fully consistent with predicted trends based on current estimates of Saturn's gravity field [6]. We may therefore use Eq. 1 to determine how long ago the C-ring was a simple inclined sheet: Julian Date 2445598±40, or Day 263±40 of 1983 [9]. This is within a year of the inclined sheet epoch derived from the previously observed temporal variations in the D-ring's corrugation wavelength [1], and the difference between the two estimates may be attributed to the excess variance in the D-ring wavelength estimates derived from images taken in different viewing geometries [1]. It is therefore reasonable to conclude that the corrugations in both the C and D rings were generated by the same ring-tilting event.

Saturn was near solar conjunction during the latter half of 1983, and thus could not be seen clearly from Earth. Archived images therefore cannot provide direct information about any event that might have caused the rings to become tilted relative to Saturn's gravitational equator. However, any acceptable scenario must be able to produce a tilt across a wide swath of the ring in a short period of time compared to the local orbital precession periods (which range between two weeks to one month). Preliminary calculations suggest that Saturn's equator is unlikely to shift appropriately due to either external torques on Saturn or mass redistribution within the planet (see SOM text 6). Furthermore, recent analyses of Galileo data indicate that Jupiter's rings became tilted around the time comet Shoemaker-Levy 9 struck the planet in 1994 [3]. We therefore investigate scenarios in which the rings became tilted relative to Saturn's equator plane due to interplanetary debris impacting the rings in 1983.

The estimated corrugation amplitudes in the C ring (Fig. 2a) indicate that the entire C ring was initially tilted relative to Saturn's equator plane by an angle $\delta\theta$ between $2*10^{-8}$ and $3*10^{-7}$ radians. Assuming a ring surface mass density of ~5 g/cm^2 (see above), the ring's angular momentum would need to re-orient by $\delta L_r \sim 10^{23}$ kg m^2/s to produce this tilt. While a reasonably dense (~ 1 g/cm^3) 1-km-wide object traveling at typical impact speeds through the rings (~40 km/s, comparable to

the escape speed from Saturn) would carry sufficient angular momentum to produce the required δL_r, it is unlikely that an intact comet or meteoroid could have produced a feature as radially extensive as the observed corrugation. A compact object ∼1 km across passing through the C ring would only interact with a small patch of the rings containing $\sim 10^{-3}$ the mass of the impactor, so any debris from this collision would follow essentially the same trajectory as the pre-impact projectile. Thus most of the incoming object's momentum would escape in the debris from the collision and not be imparted to the rings, and no large-scale tilt would be established. However, if the rings encountered a diffuse cloud of debris instead of a single solid object, then material would have rained down across a range of radii, producing a tilt that could ultimately form an extensive corrugation. The incoming debris would also interact with a much larger area of the rings and a much greater mass of ring material, so more of the momentum carried by the debris should remain in the ring instead of departing from the Saturn system. Such a scenario could even explain the differences in the corrugation amplitudes between the C and D rings. Assuming the momenta from the incoming particles are efficiently transferred to the rings (see SOM text 7), the tilt induced by a given debris flux should be directly proportional to the ring particles' aggregate cross section and inversely proportional to their total mass. The larger amplitude of the D-ring corrugation could therefore arise simply because of the sub-millimeter-wide particles in the D ring [1] have much higher surface-area-to-volume ratios than the centimeter-to-meter-sized C-ring particles [10].

The viability of this explanation for the ring's initial tilt can be evaluated by estimating the total debris mass required to produce the observed corrugations. For rings of modest optical depth like the C ring, the angular momentum delivered into the rings by a debris cloud of mass m_c can be expressed as:

$$L_c = D_F \tau m_c v_c r, \tag{4}$$

where v_c is the mean impact speed of the incoming material, r and τ are the orbital radius and normal optical depth of the ring and D_F is a dimensionless parameter that depends on the longitudinal distribution of the impacting material. For a homogeneous debris cloud, $D_F \sim 0.1$ for a wide range of plausible approach trajectories and speeds (see SOM text 7), and could be higher if the cloud has substantial substructure. Assuming D_F lies between 1 and 0.01, and further stipulating that $L_c \simeq \delta L_r \sim 10^{23}$ kg m^2/s, $v_c \simeq 40$ km/s and $\tau \sim 0.1$ (see Fig. 2e), we find that the total mass of the debris cloud would need to be 10^{11}-10^{13} kg in order to produce the observed C-ring corrugation.

Debris clouds with masses of order 10^{12} kg were produced during the break-up of Shoemaker-Levy 9 in 1992 [11, 12] and the major outburst of comet 17P/Holmes in 2007 [13]. The rate at which Saturn would encounter such massive clouds is quite uncertain, but let us consider the

specific scenario where a 1-km wide comet nucleus was captured into orbit around Saturn, broke apart during a close periapse passage (due to planetary tides or a collision with the rings), producing $\sim 10^{12}$ kg of debris on bound orbits that crashed into the rings on a later periapse [14]. While the rate at which captured cometary debris impacts Saturn has not yet been thoroughly investigated in numerical simulations, existing studies indicate that roughly 4% of the comets that impact Jupiter had previously passed close enough to the planet to be disrupted [15], the impact flux at Saturn is about 40% the flux at Jupiter [16, 17], and the fraction of impactors on bound orbits is about an order of magnitude less for Saturn than it is for Jupiter [18, 19, 20]. Together, these results indicate that Saturn should encounter debris clouds derived from comets disrupted by previous planetary encounters at a rate that is roughly 0.2% of Jupiter's impact rate. The 2009 detection of a fresh impact scar at Jupiter suggests that 1-km-wide objects may strike Jupiter as often as once a decade [21]. In this case, the clouds of orbiting debris created by the disruption of a 1-km-wide comet should rain down on Saturn's rings once every 5,000-10,000 years. The probability that debris from a previously-disrupted comet would hit Saturn's rings in the last 30 years would then be between roughly 1% and 0.1%, which is not very small. Such scenarios therefore provide a reasonable explanation for the origin of the observed corrugation in Saturn's C ring.

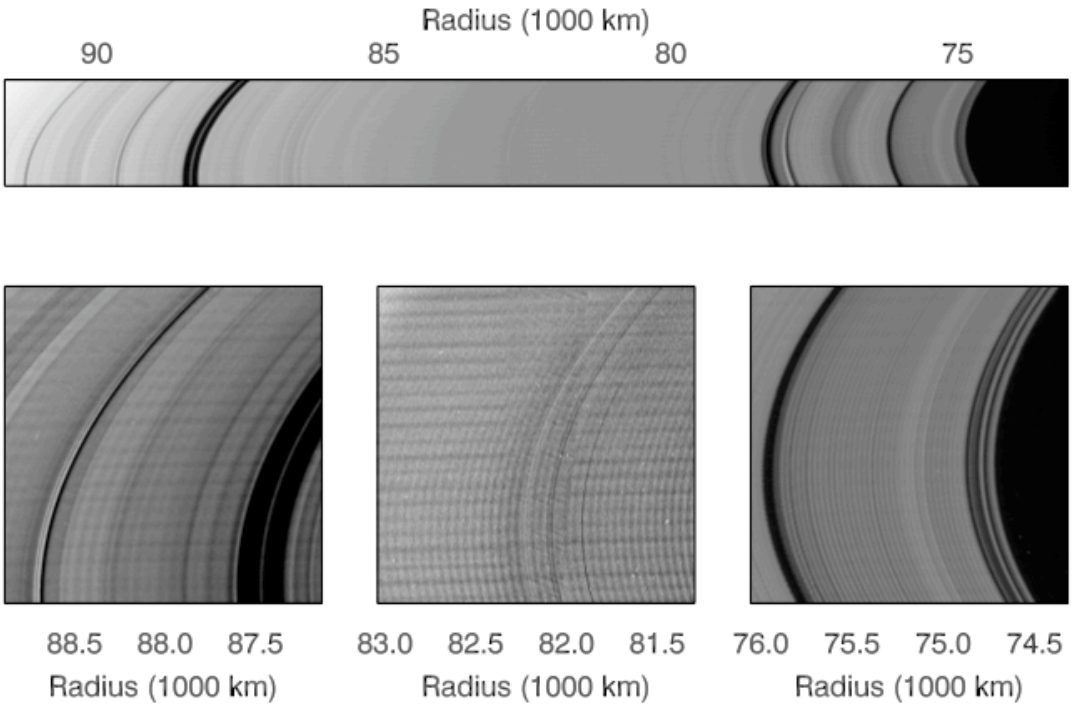

Figure 1: Mosaic of images of Saturn's C ring obtained during Cassini's orbit 117, along with close-ups of selected radial regions showing the periodic bright and dark bands that permeate the entire C ring. The contrast has been adjusted in each close-up image to better show the periodic structure. Horizontal bands within these close-ups are camera artifacts. [22]

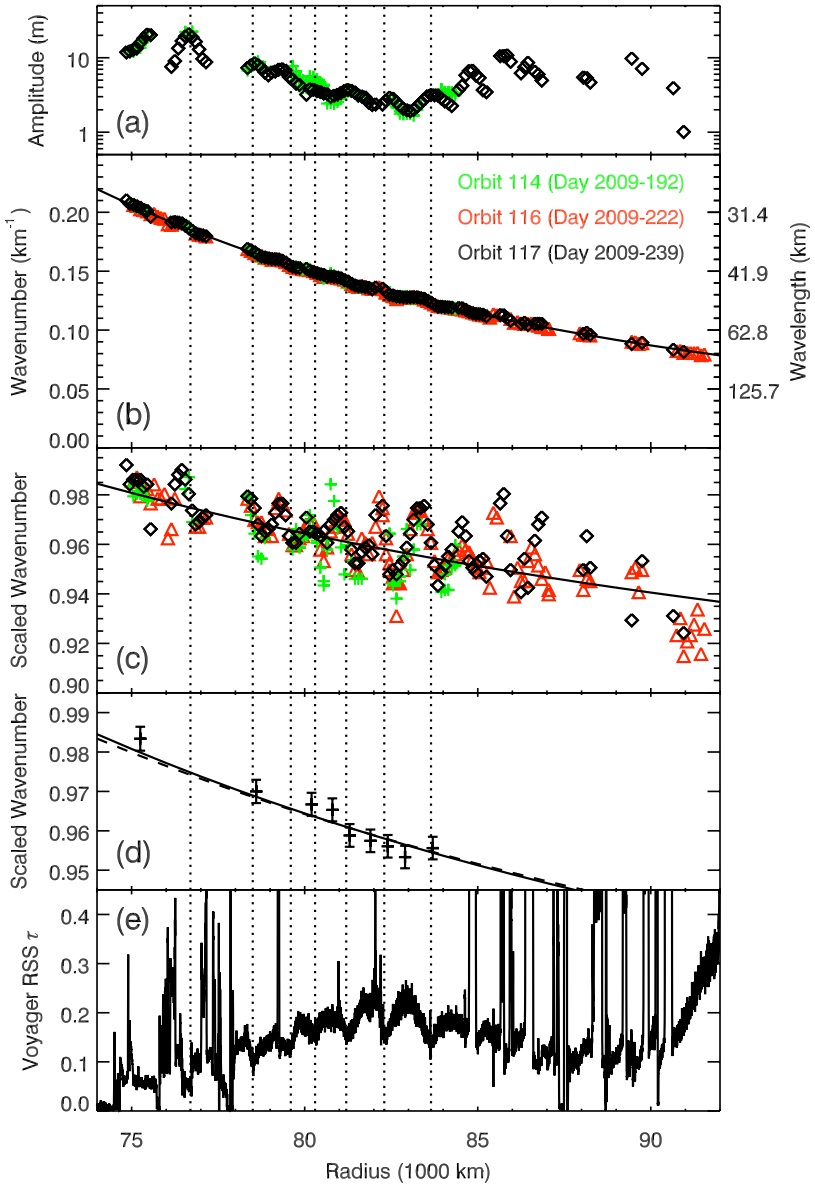

Figure 2: Corrugation parameters versus radius in the rings (distance from Saturn's spin axis) derived from three observations taken on three different Cassini orbits around the time of Saturn's equinox (see SOM text 1 and 2 for analysis procedures): (a) corrugation amplitude A_z, (b) corrugation wavenumber k_z and (c) scaled corrugation wavenumber $k'_z = k_z/k_o * (r/r_o)^{9/2}$, where $k_o = (2\pi/40)\text{km}^{-1}$ and $r_o = 80{,}000$ km are constants chosen to normalize k'_z to approximately unity at equinox. In these plots, each data point is computed from a Fourier analysis of a 500-km-wide ring region, so adjacent data points from the same observation, which are separated by only 100 km, are not independent. No amplitudes are plotted for the Orbit 116 data because the extremely low Sun-opening angle during these observations complicates the photometry (see SOM text 2). (d) Estimates of the rescaled corrugation wavenumber on JD 2455054 at locations in the ring where the finite mass of the ring is negligible (see SOM text 5). The solid curves in panels (b), (c) and (d) are the predicted wavenumber of a vertical corrugation produced by differential nodal regression of an inclined ring that existed at JD 2445598, assuming the standard model of Saturn's gravity field [6] with $J_n = 0$ for $n > 8$. In panel (d), the dashed curve shows a similar prediction assuming $J_8 = 0$ instead of $J_8 = -0.00001$ (e) Normal optical depth profile of the C ring measured by the Voyager Radio Science Subsystem (obtained from the Planetary Data System rings node).

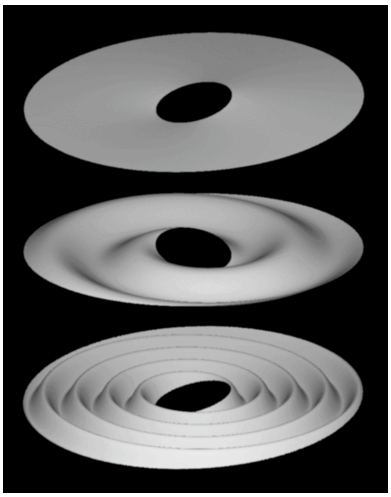

Figure 3: Cartoon representation of how differential nodal regression produces a vertical corrugation from an initially inclined ring. The top image shows a simple inclined ring (the central planet is omitted for clarity), while the lower two images show the same ring at two later times, where the orbital evolution of the ring particles has sheared this inclined sheet into an increasingly tightly-wound spiral corrugation.

Supporting Text 1: Data-Reduction Techniques

Imaging data reduction

Our study is based on radial brightness profiles derived from images obtained by the Narrow-Angle Camera (NAC) of the Imaging Science Subsystem (ISS) onboard the Cassini Spacecraft [22]. Images from the observation sequences in Table S1 were calibrated using routines that remove instrumental backgrounds, flat-field the images and convert the data numbers into I/F, a standardized measure of reflectivity that is unity for a Lambertian surface viewed at normal incidence [22]. Individual images are then geometrically navigated using stars in the field of view and fiducial ring features. Finally, the brightness data are averaged over a range of longitudes to determine the mean brightness of the ring versus radius.

Fourier analysis of radial profiles

The relevant brightness profiles all show periodic brightness variations. Fourier analysis is the most obvious way to isolate and quantify these structures. However, since the wavelength of this pattern is a continuous function of radius, and furthermore because other structures are present in the ring besides the corrugation, the radial profiles need to be processed prior to computing the Fourier transform.

First, the radial profile is high-pass filtered to remove any background slopes or broad-scale trends in the data that could complicate the Fourier analysis. This is done by subtracting a boxcar-smoothed version of the radial profile from the original data. The smoothing length scale is chosen to be 200 km, which is 2-5 times the wavelength of the observed pattern. The results of this analysis do not change significantly so long as this parameter is not too small.

Table S1: Overview of the Geometry of the C-ring observations

Orbit[a]	Observation[b]	Obs. Date	Phase Angle	$B^c_\odot$	B^d_C	ϕ^e_{obs}	$\phi^f_\odot$	ϕ^g_C
100	MNRNGSHAD004	2009-012	71.9°-79.2°	-3.24°	66.6°-63.6°	343.1°-93.1°	218.1°	256.5°-276.5°
114	MNRNGSHAD004	2009-192	23.7°-24.6°	-0.47°	22.9°-24.0°	135.9°-141.1°	223.6°	216.1°-217.0°
116	EQXSHADOW001	2009-222	152.1°-151.5°	-0.01°	-4.1 °- -4.3°	102°-112°	224.5°	21.6°-22.1°
117	EQXSHADOW013	2009-239	11.6°-9.8°	+0.26°	7.1°-7.9°	303°-312°	225.1°	226.0°-231.1°

[a] Orbit of Cassini around Saturn
[b] Name of observation sequence, individual filenames are given in Tables S2 and S3.
[c] Solar elevation angle above the ring plane.
[d] Spacecraft elevation angle above the ring plane.
[e] Inertial longitude (relative to the rings' ascending node on J2000) of the observed point in the ring.
[f] Inertial longitude of the sun in the rings.
[g] Inertial longitude of the spacecraft in the rings. Note longitude ranges of orbit 116 and orbit 117 data are for the portions of images used in the radial scans.

Second, the measured radial positions r in the ring are converted into a re-scaled distance parameter d:

$$d = \frac{2}{7}\frac{r}{\lambda_o}\left(\frac{r_o}{r}\right)^{9/2}, \tag{S1}$$

where λ_o and r_o are constants. The "rescaled wavelength" of a periodic structure measured in this transformed coordinate system is:

$$\lambda' = \frac{\lambda}{\lambda_o}\left(\frac{r_o}{r}\right)^{9/2}, \tag{S2}$$

where λ is the true radial wavelength. Based on the observations discussed in the main text, λ scales approximately as $r^{9/2}$, so λ' is approximately constant. This transformation therefore allows Fourier analyses to be performed on longer stretches of data without encountering difficulties associated with position-dependent wavelength drifts, enabling us to obtain more precise wavelength measurements. For this particular analysis, the parameters in the transformation are chosen to be $\lambda_o = 40$ km and $r_o = 80{,}000$ km. This normalizes the rescaled wavelength λ' to be approximately unity throughout the C ring during the equinox epoch. We also define a re-scaled wavenumber $k' = 1/\lambda'$, which is also approximately unity during the equinox epoch.

After high-pass-filtering the data and re-scaling the radius scale, an over-resolved Fourier spectrum of the selected data is computed by evaluating the Fourier transform for a tightly spaced array of λ' values ($\delta\lambda' = 0.001$). These spectra typically show a strong peak near $\lambda' = 1$. This peak is then fitted to a Guassian in order to obtain estimates of the pattern's wavelength and amplitude. Only data having λ' within ± 0.1 of the peak location and above 0.5 of the peak amplitude are included in the fit. The fitting routine then returns the following parameters:

- The mean orbital radius of the analyzed data set.
- The median I/F of the analyzed data $M_{I/F}$.
- The location of the peak in the Fourier spectrum, which is an estimate of λ'.
- The amplitude $A_{I/F}$ of the pattern, derived from the peak amplitude of the Fourier spectrum.
- The Gaussian width of the peak in the Fourier spectrum σ'_λ, which is a useful tool for determining the quality of the wavelength data.
- The standard deviation of the high-pass-filtered data $s_{I/F}$, which is another means to evaluate the quality of the wavelength data.

Note that the fractional amplitude of the brightness variations is given by $A_{I/F}/M_{I/F}$.

Evaluating the quality of the wavelength measurements

While the high-pass filtering and re-scaling help produce robust wavelength estimates, we still must cope with various sharp features, such as gap edges, plateau edges, ringlets, stars or cosmic rays, that may affect the wavelength estimates. In some cases (such as our analysis of the observations from Orbit 100), we deal with these issues by judiciously selecting the regions to analyze. However, for the equinox observations covering a large radial range in the C ring, we wanted to be able to exclude data affected by small-scale features automatically. This was accomplished using the following criteria to evaluate the quality of the wavelength measurements:

- The re-scaled wavelength λ', which should not deviate too much from unity.
- The re-scaled wavelength spread σ'_λ. This is a measure of the reliability and precision of the wavelength measurement, and should not be too large.
- The "excess variance" of the data, defined as $(s_{I/F} - A_{I/F}/\sqrt{2})/A_{I/F}$, where $s_{I/F}$ is the standard deviation of the de-trended radial profile and $A_{I/F}$ is the estimated amplitude of the periodic brightness variations. This is a measure of the strength of any non-sinusoidal features in the data, and should not be too large.

Figure S1 shows histograms of these parameters for wavelength measurements derived from Fourier analyses of 500-km wide regions of the radial scans derived from the various equinox observations. Based in part on inspection of these histograms, we chose to exclude all data with λ' less than 0.95 or greater than 1.10, σ'_λ greater than 0.09, and excess variance greater than unity. We also deliberately exclude regions near the (non-circular) ringlets at 77,860, 87,500, 88,710 and 90,160 km. These cuts eliminate the outliers in the distribution and therefore allow us to produce reliable plots of wavelength versus radius without selecting radial ranges explicitly by hand. The data that pass these criteria are plotted in Fig. 2.

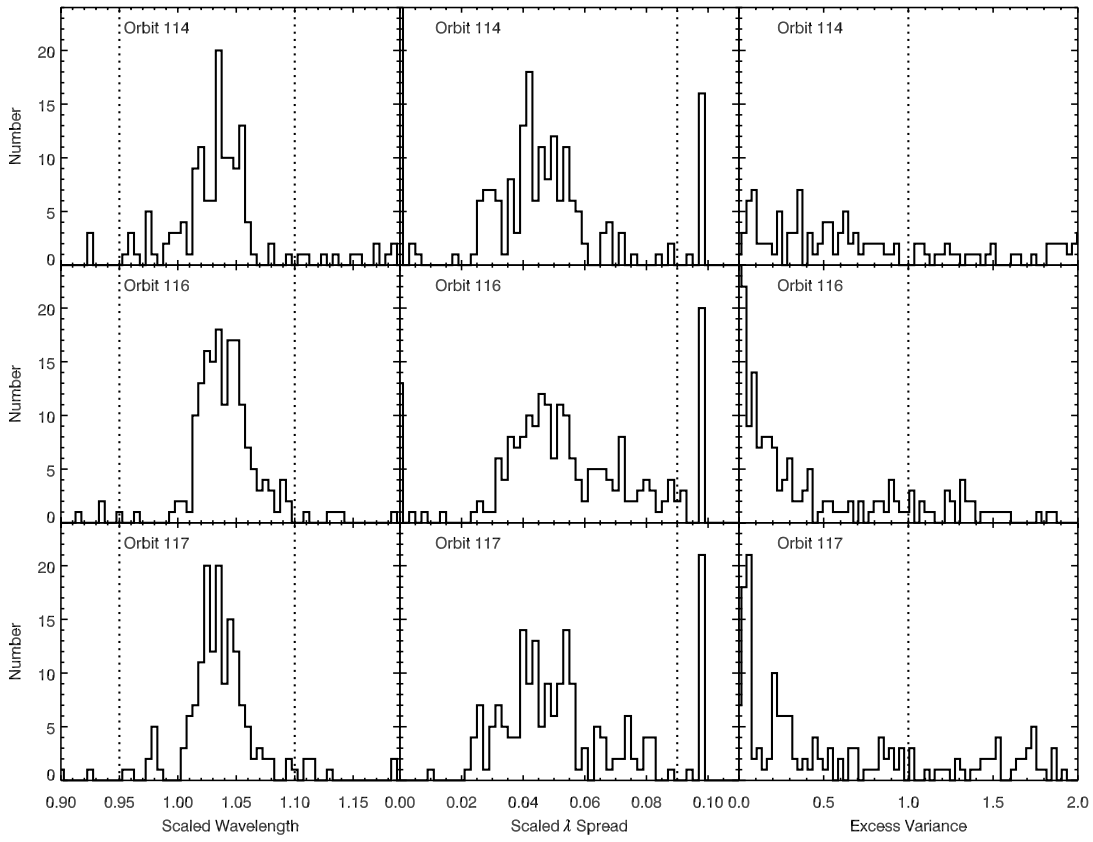

Figure S1: Histograms of the various quality-of-fit parameters for wavelength measurements derived from Fourier analyses of 500-km-wide regions of the radial scans derived from the Orbit 114, 116 and 117 sequences. The left-hand column shows the scaled wavelength values. The middle column displays the scaled wavelength spread values σ'_λ, and the right-hand column shows the data's "excess variance", defined as $(s_{I/F} - A_{I/F}/\sqrt{2})/A_{I/F}$, where $s_{I/F}$ is the standard deviation of the de-trended data, and $A_{I/F}$ is the amplitude of the periodic brightness variation. The dotted lines indicate the limits on the scaled wavelengths and the upper bounds on the scaled wavelength spreads and excess variances used to select reliable wavelength measurements.

Supporting Text 2: Photometry of corrugated rings

To first order, a ring's apparent surface brightness S is given by the standard single-scattering formulae [23] for cases where the light source and observer are on the same side of the ring (reflected light):

$$S_r = S_o \frac{\mu_0}{\mu_0 + \mu}[1 - e^{-\tau/\mu_{eff}}], \tag{S3}$$

and where the light source and receiver are opposite sides of the ring (transmitted light):

$$S_t = S_o \frac{\mu_0}{\mu_0 - \mu}[e^{-\tau/\mu_0} - e^{-\tau/\mu}]. \tag{S4}$$

In these expressions, S_o is a factor that depends on the ring's intrinsic albedo and phase function, τ is the ring's optical depth, μ and μ_0 are the cosines of the incidence and emission angles, and $\mu_{eff} = \mu\mu_0/(\mu + \mu_0)$. A corrugation in the ring will cause the photometrically relevant direction cosines μ and μ_0 to vary with radius, and thereby generate brightness variations.

Consider a vertically corrugated ring in which the ring's vertical displacement z is a simple sinusoidal function of the radius r:

$$z = A_z \sin(k_z r), \tag{S5}$$

where A_z and $k_z = 2\pi/\lambda_z$ are the amplitude and the wavenumber of the corrugation, respectively. Also, imagine that Cassini observes this corrugated ring from an angle B_C above the ring plane and an azimuthal angle of ϕ'_C relative to the local radial direction. Similarly, say that the sun illuminates the rings from an angle $B_\odot$ above the rings and is located at an azimuth $\phi'_\odot$. In a Cartesian coordinate system where the x axis is in the local radial direction, the y axis points in the local azimuthal direction, and the z axis points vertically, the local surface normal to the warped surface is:

$$\hat{\mathbf{n}} = \frac{\hat{\mathbf{z}} - (A_z k_z \cos k_z r)\hat{\mathbf{x}}}{\sqrt{1 + (A_z k_z \cos k_z r)^2}}, \tag{S6}$$

while the unit vectors aligned with the incident and emitted light rays from the corrugated surface are:

$$\hat{\mathbf{i}} = \cos B_\odot \cos \phi'_\odot \hat{x} + \cos B_\odot \sin \phi'_\odot \hat{y} + \sin B_\odot \hat{z} \tag{S7}$$

and

$$\hat{\mathbf{e}} = \cos B_C \cos \phi'_C \hat{x} + \cos B_C \sin \phi'_C \hat{y} + \sin B_C \hat{z}. \tag{S8}$$

The relevant direction cosines can therefore be expressed as:

$$\mu_0 = |\hat{\mathbf{n}} \cdot \hat{\mathbf{i}}| = |\sin B_\odot| \left| \frac{1 - \cot B_\odot \cos \phi'_\odot (A_z k_z \cos k_z r)}{\sqrt{1 + (A_z k_z \cos k_z r)^2}} \right| \tag{S9}$$

and

$$\mu = |\hat{\mathbf{n}} \cdot \hat{\mathbf{e}}| = |\sin B_C| \left| \frac{1 - \cot B_C \cos \phi'_C (A_z k_z \cos k_z r)}{\sqrt{1 + (A_z k_z \cos k_z r)^2}} \right|. \tag{S10}$$

(Note that in the limit where corrugations are tiny ($A_z \simeq 0$), then $\mu_0 \simeq |\sin B_\odot|$ and $\mu \simeq |\sin B_C|$, as expected.)

Inserting these expressions for μ and μ_0 directly into Eqs. S3 and S4 yields rather complicated expressions for the surface brightness. It is therefore more useful to consider limiting cases appropriate to the images analyzed here, which were taken close to equinox. Thus $|B_\odot|$ is sufficiently small that we can assume that $\mu_0 << \mu$ and that $e^{-\tau/\mu_0} \simeq 0$. Furthermore, the images of the C ring discussed here were either taken on the lit side of the rings, or at sufficiently high values of B_C that $e^{-\tau/\mu}$ can be approximated as unity (see Table S1). In these situations, the surface brightness formulae may be approximated as:

$$S_r \simeq S_t \simeq S_C = S_o \frac{\mu_0}{\mu}. \tag{S11}$$

Substituting in the above expressions for μ and μ_0 yields:

$$S_C = S_o \left| \frac{\sin B_\odot}{\sin B_C} \right| \left| \frac{1 - \cot B_\odot \cos \phi'_\odot (A_z k_z \cos k_z r)}{1 - \cot B_C \cos \phi'_C (A_z k_z \cos k_z r)} \right|. \tag{S12}$$

The brightness variations should therefore have the same characteristic wavelength as the underlying corrugation. Furthermore, the fractional brightness variations are (to first order in $A_z k_z$):

$$F_C = A_z k_z |\cot B_\odot \cos \phi'_\odot - \cot B_C \cos \phi'_C|. \tag{S13}$$

Note that since $|B_\odot| << |B_C|$, we expect the first term to dominate, so the fractional amplitude of the brightness variations should be proportional to $|\cot B_\odot \cos \phi'_\odot|$.

A sequence of images covering a wide range of longitudes in the C ring taken six months prior to equinox (during Cassini Orbit 100) clearly demonstrates that the amplitude of the brightness variations is proportional to $|\cos \phi'_\odot|$ (see Fig. S2 and Table S2). This provides strong evidence that these periodic brightness variations are indeed due to a vertical corrugation.

Rough estimates of the corrugation amplitude can be obtained from the observed amplitudes and wavelengths of the brightness variations using the above model (see Fig. 2a). However, it is

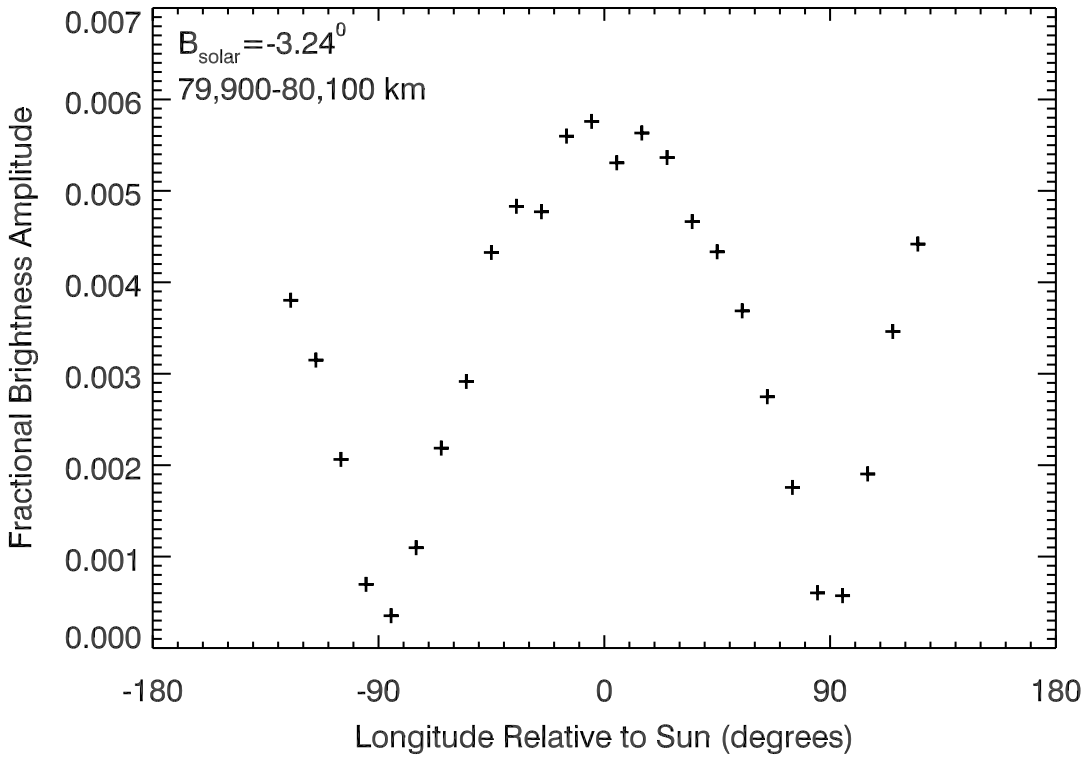

Figure S2: Fractional amplitude of brightness variations between 79,900 and 80,100 km from Saturn's center versus longitude relative to the Sun $\phi'_\odot$ derived from a series of observations taken six months prior to equinox, when $B_\odot = -3.24°$ (see Table S2). The amplitude clearly scales like $|\cos\phi'_\odot|$ as predicted for a vertical corrugation.

important to realize that this simple model does not include the effects of Saturn-shine or the ring's finite thickness, both of which are likely to be important given the low solar elevation angles and the small corrugation amplitudes involved. Thus the derived estimates of the corrugation amplitude A_z may contain significant systematic errors. Indeed, the corrugation amplitudes derived from the data in Fig. S2 differ from those derived from the Orbit 114 and 117 data shown in Fig. 2a by almost a factor of two. More complex and detailed photometric modeling will therefore be needed to obtain accurate and robust estimates of the corrugation amplitudes.

Table S2: Orbit 100 measurements of brightness variations in the range 79,900-80,100 km ($B_\odot = -3.24°$).

Image Name	$\phi_{obs} - \phi_{Sun}$	Fractional Amplitude	Wavelength (km)
N1610490312	+125°	0.0042	42.4
N1610490912	+115°	0.0034	42.4
N1610491512	+105°	0.0019	41.6
N1610492112	+95°	0.0006	38.7
N1610492712	+85°	0.0006	43.2
N1610493312	+75°	0.0018	42.7
N1610493912	+65°	0.0029	43.1
N1610494512	+55°	0.0038	42.7
N1610495112	+45°	0.0044	43.1
N1610495712	+35°	0.0047	42.8
N1610496312	+25°	0.0053	43.4
N1610496912	+15°	0.0055	43.2
N1610497512	+5°	0.0051	43.0
N1610498112	-5°	0.0054	43.0
N1610498712	-15°	0.0052	42.5
N1610499312	-25°	0.0043	41.4
N1610499912	-35°	0.0043	42.1
N1610500512	-45°	0.0039	42.7
N1610501112	- 55°	0.0027	41.8
N1610501712	-65°	0.0021	41.6
N1610502312	-75°	0.0011	39.8
N1610502912	-85°	0.0004	37.3
N1610503512	-95°	0.0008	44.1
N1610504112	-105°	0.0023	43.2
N1610504712	-115°	0.0036	43.0
N1610505312	-125°	0.0043	43.2

Supporting Text 3: Corrugation wavelengths and the modulations induced by a finite ring mass

Say a ring became inclined to Saturn's equatorial plane at a time t_i. At this time, all the ring-particles' orbits have their ascending nodes at the same longitude, which we can set to zero without loss of generality. Thus $\Omega(r, t_i) = 0$ at all radii. However, if the ring is observed at a later time t_f, then the ring will not appear as a simple inclined sheet because the nodes of the particles' orbits will regress at a radially-dependent rate $\dot{\Omega}(r)$. If the particles' orbits are sufficiently circular that collisions between particles with different semi-major axes are unable to dissipate orbital inclinations and flatten the ring, and if the nodal regression rate is determined entirely by Saturn's unchanging gravitational field (see below), then at time t_f, the node location at any given radius is simply $\Omega(r, t_f) = (t_f - t_i) * \dot{\Omega}(r)$. In general, $|\dot{\Omega}|$ is a monotonically decreasing function of radius r [4], so the longitude of ascending node forms an increasingly tightly wound spiral as t_f increases (see Fig. 3). A radial cut through this structure will therefore show the vertical position of the ring oscillating up and down as a function of radius, producing the desired corrugation. The wavelength λ_z of this corrugation corresponds to a radial distance Δr over which the node's longitude has cycled through 360° (i.e., $\Delta\Omega = 2\pi$), so the wavenumber $k_z = 2\pi/\lambda_z$ is given by the expression:

$$k_z = \left| \frac{\partial}{\partial r} \Omega \right| = \left| \frac{\partial}{\partial r} \int_{t_i}^{t_f} \dot{\Omega} dt \right|, \tag{S14}$$

where $\dot{\Omega}$ is the nodal regression rate. If the ring were massless, the precession rate would be entirely due to Saturn's gravity field, given by the difference in the epicyclic frequencies:

$$\dot{\Omega}(r) = \dot{\Omega}_o(r) = n - \nu, \tag{S15}$$

where n is the particle's mean motion and ν is the vertical epicyclic frequency [4]. In this case, the precession rate is a constant in time and the integral is trivial. Thus the wavenumber is just:

$$k_z^o = \left| \frac{\partial \dot{\Omega}_o}{\partial r} \right| (t_f - t_i). \tag{S16}$$

And, assuming that J_2 dominates the nodal regression rates, this means $k_z^o \sim r^{-9/2}$, and $\lambda_z^o = 2\pi/k_z^o \sim r^{9/2}$, as observed (see main text).

Now consider the case where the ring has a finite surface mass density σ that can vary with radius. This will change the precession rates in the ring by a small amount, which can be computed

using the dispersion relation for free vertical waves derived in [24, Eq. 84]:

$$(\dot{\Omega} - n)^2 = \nu^2 + 2\pi G\sigma|k_z|. \tag{S17}$$

(Note we assume a $m = 1$ disturbance and change [24]'s notation to match our own). Solving this equation for $\dot{\Omega}$, we find (taking the lower frequency solution):

$$\dot{\Omega} = n - \nu\sqrt{1 + \frac{2\pi G\sigma}{\nu^2}|k_z|}. \tag{S18}$$

If we now assume that $2\pi G\sigma|k_z| << \nu^2$, which is valid for the C ring corrugations throughout their history, then we may approximate the above expression as:

$$\dot{\Omega} = n - \nu - \frac{\pi G\sigma}{\nu}|k_z| = \dot{\Omega}_o - \frac{\pi G\sigma}{\nu}|k_z|. \tag{S19}$$

Again, assuming that the second term in the above expression is a small perturbation, then we may approximate $|k_z|$ in this expression as simply $|\partial\dot{\Omega}_o/\partial r|(t - t_i)$:

$$\dot{\Omega} = \dot{\Omega}_o - \frac{\pi G\sigma}{\nu}\left|\frac{\partial\dot{\Omega}_o}{\partial r}\right|(t - t_i). \tag{S20}$$

Inserting this expression into Eq. S14, we get

$$k_z = \left|\frac{\partial}{\partial r}\int_{t_i}^{t_f}\left[\dot{\Omega}_o - \frac{\pi G\sigma}{\nu}\left|\frac{\partial\dot{\Omega}_o}{\partial r}\right|(t - t_i)\right]dt\right|. \tag{S21}$$

Now we may evaluate the integral, take the derivative, and pull out a factor k_z^o (see Eq. S16) to obtain the expression:

$$k_z = k_z^o\left(1 - \frac{\pi G}{2\nu}\frac{\partial\sigma}{\partial r}(t_f - t_i) + \frac{\pi G\sigma}{2\nu^2}\frac{\partial\nu}{\partial r}(t_f - t_i) + \frac{\pi G\sigma}{2\nu}\left|\frac{\partial^2\dot{\Omega}_o/\partial r^2}{\partial\dot{\Omega}_o/\partial r}\right|(t_f - t_i)\right). \tag{S22}$$

Thus the ring's mass induces three correction terms to the wavenumber. We may simplify the last two of these terms by recalling that, to first order, $\nu \propto r^{-3/2}$ and $\dot{\Omega}_o \propto r^{-7/2}$, so the derivatives in these two terms can be evaluated and then the terms combined to yield:

$$k_z = k_z^o\left(1 - \frac{\pi G}{2\nu}\frac{\partial\sigma}{\partial r}(t_f - t_i) + \frac{\pi G}{2\nu}\frac{3\sigma}{r}(t_f - t_i)\right). \tag{S23}$$

In other words, the fractional variations in the corrugation wavenumber induced by the ring's own

gravity are:

$$\frac{\delta k_z}{k_z} = \frac{\pi G}{2\nu}\left(-\frac{\partial \sigma}{\partial r} + \frac{3\sigma}{r}\right)(t_f - t_i). \tag{S24}$$

Supporting Text 4: Quantitative analysis of wavelength residuals induced by the C-ring's finite mass density

We can estimate the mass density that the C ring would need in order to produce the observed wavenumber residuals if we assume the ring's optical depth is strictly proportional to its surface mass density, i.e., the opacity τ/σ is constant. In this case we can use the Voyager RSS optical depth profile obtained from the Planetary Data System to compute the product of the opacity times the predicted wavenumber residuals $(\tau/\sigma)\delta k_z/k_z$ and compare these numbers to the observed deviations from the predicted trend. Since τ/σ may not be constant over regions containing dramatic variations in the optical depth [25], we restrict this analysis to the region between 78,000 km and 84,000 km, where the optical depth variations are relatively subtle. As shown in Fig. S3, the observed wavenumber residuals are reasonably well correlated with the average values of $(\tau_{RSS}/\sigma)(\delta k_z/k_z)$ derived from the optical-depth profile. This is consistent with τ_{RSS}/σ being approximately constant. Fitting a line to these data, we can estimate the radio opacity in this part of the C ring to be $\tau_{RSS}/\sigma = 0.034 \pm 0.005$ cm^2/g (which would correspond to an optical opacity of 0.017 cm^2/g) and implies that the surface mass density of the middle C ring would need to be 3-6 g/cm^2 in order to produce the observed wavenumber residuals. These values are reasonably consistent with mass density estimates derived from scattering of the Voyager radio signals [7] and several unidentified density and/or bending waves in this region (assuming the number of arms in some of these waves exceeds two) [8]. While this mass density is several times higher than published estimates derived from identifiable waves in the C ring [26, 27, 8], both these features are found in the inner C ring, where the background optical depth is somewhat lower than it is in the middle C ring. The mass density required to produce the observed residuals in the corrugation's wavenumber therefore does not seem unreasonable. Furthermore, if we assume the C-ring ramp has an opacity similar to that of the middle C-ring, this would account for the 1-2% residuals in the wavenumbers beyond 90,000 km seen in Fig. 2c.

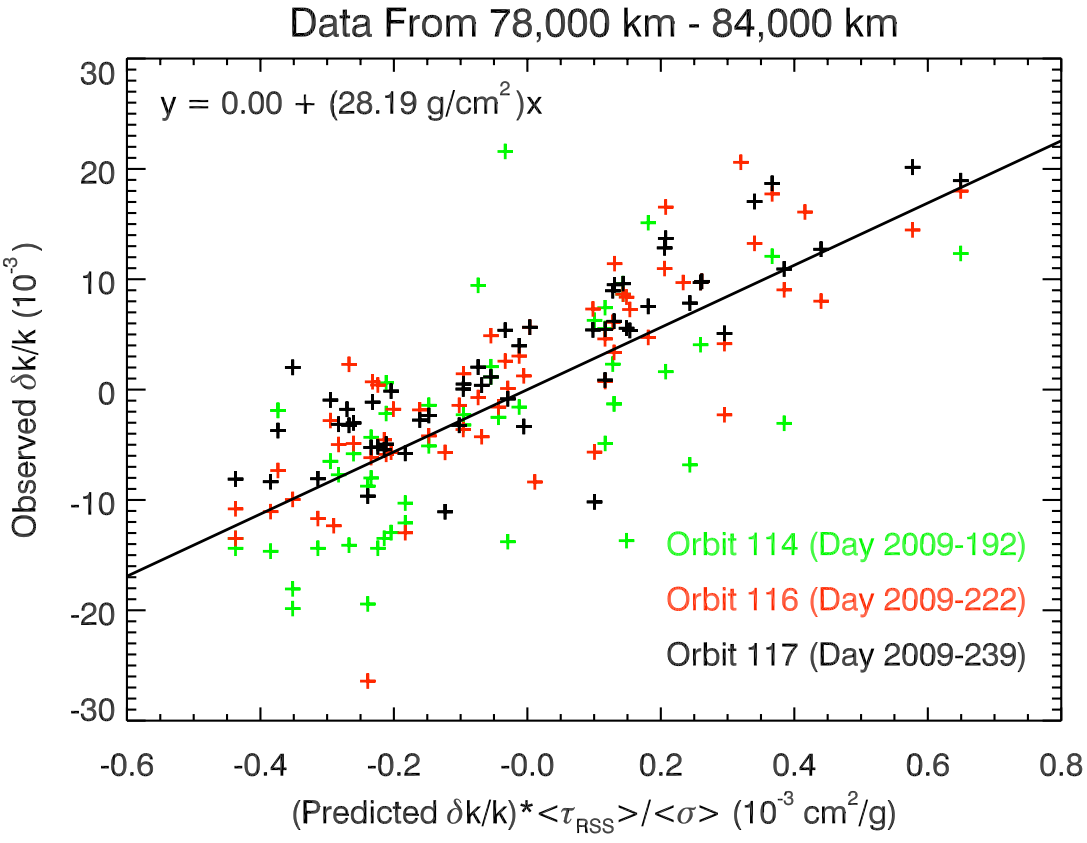

Figure S3: Plot of the observed wavenumber residuals $\delta k_z/k_z$ versus the predicted $(\tau_{RSS}/\sigma)\delta k_z/k_z$ assuming the mass density is directly proportional to the optical depth. The data come from the region between 78,000 km and 84,000 km from Saturn center, and each point derives from an analysis of a region 500 km across, with central values sampled every 100 km. The data points are therefore correlated. The slope of a linear fit to these data implies an opacity $\tau_{RSS}/\sigma = 0.034 \pm 0.005$ cm^2/g (the error bar accounts for the oversampling in the data by rescaling the fit error by $\sqrt{5}$).

Supporting Text 5: Estimates of C-ring corrugation wavelengths in selected regions

Table S3: Selected C-ring corrugation wavelength estimates

Radius (km)	Orbit 116 Image	Orbit 117 Image	Orbit 116 λ_z (km)	Orbit 117 λ_z (km)	Equinox λ_z^a (km)	Predicted $\delta k_z/k_z^b$
75250±200	N1628587518	N1630093134	30.92	30.79	30.88±0.10	+0.00113
78600±250	N1628588163	N1630094064	38.09	38.01	38.08±0.12	-0.00033
80200±250	N1628588163	N1630094529	41.75	41.87	41.85±0.13	-0.00194
80800±250	N1628588163	N1630094529	43.25	43.25	43.33±0.13	-0.00006
81300±250	N1628588163	N1630094529	44.86	44.77	44.86±0.13	-0.00014
81900±250	N1628588163	N1630094529	46.54	46.23	46.43±0.14	+0.00018
82400±250	N1628588812	N1630094994	47.70	47.79	47.79±0.14	+0.00085
82900±250	N1628688812	N1630094994	49.25	49.16	49.25±0.15	+0.00079
83700±250	N1628688812	N1630094994	51.23	51.28	51.30±0.15	-0.00018

Note: Orbit 114 data are not used in this analysis because the corrugation signal was smaller relative to background brightness trends, leading to a larger scatter in the wavelength measurements.

[a] The estimate is the average of the Orbit 116 wavelength and the Orbit 117 wavelength rescaled by a factor of 1+ (17/9450) to account for the evolution of the corrugation wavelength in the 17 days between the observations. The error bars are those based on the scatter of the differences between these two numbers among the different measurements.

[b] Predicted $\delta k_z/k_z$ is computed assuming a radio opacity of 0.034 cm^2/g, see SOM text 4.

Supporting Text 6: Shifting Saturn's equator plane

In principle, changes in Saturn's gravitational field could move the planet's gravitational equator plane out from under the rings, giving a wide region of the rings a finite inclination relative to the planet. However, as discussed in detail below, many scenarios involving changes to the planet's spin axis or internal structure are unlikely to generate sufficiently large tilt angles over a sufficiently short timescale, and therefore do not provide viable alternatives to the ring-tilting impact events discussed in the main text.

Of course, the simplest way to change Saturn's gravitational equator by an angle $\delta\theta$ is to tilt the entire planet, but this is extremely unlikely to have occurred in the last 30 years. A change in Saturn's spin axis $\delta\theta$ corresponds to a change in the orientation of the planet's angular momentum:

$$\delta L_S = F_S M_S R_S^2 \omega_S \delta\theta, \tag{S25}$$

where F_S is a factor of order unity, M_S and R_S are the planet's mass and radius, and ω_S is the bulk spin rate. Assuming $\omega_S \sim 820°$/day (or a rotation period of ~ 10.5 hours), then the required angular momentum shift is $\delta L_S \sim 10^{31}$ kg m^2/s. Such a large change in angular momentum would require an extreme event like a collision with an object with a mass of order 10^{18} kg. (and $\sim$100 km wide assuming it had a density comparable to water ice). Such events are very unlikely to have occurred in the last century [17], so this particular scenario can be effectively ruled out as an explanation for the corrugation.

Instead of tilting the entire planet, one may consider the possibility that a shift in the mass distribution or flow fields inside Saturn changed the orientation of the planet's gravitational equator. Note that such shifts would need to happen relatively rapidly, or else the ring particles' orbits will just adiabatically track the motion of Saturn's gravitational equator. Since the nodal regression periods in the C ring are on the order of weeks, this means that the changes in the planet's mass distribution must occur in just a few days, so seasonal processes are unlikely drivers. Instead, we will consider more rapid phenomena. For example, consider a parcel of material with mass M_P rising from close to the planets's center to near its surface or sinking from the surface to near the center. In either case, this motion could tilt Saturn's equator by a factor of $\delta\theta \sim F_P M_P/(J_2 M_S)$, where F_P is a constant of order unity. To produce the required tilt $\delta\theta \sim 10^{-7}$, M_P would need to be on the order of 10^{-8} the mass of the entire planet. Alternatively, Saturn's equatorial jet could have become misaligned relative to the rest of the planet. If the jet has a mass M_J and changes its orientation by an angle $\delta\theta_J$, this will tilt the location of Saturn's gravitational equator by an angle $\delta\theta \sim F_J \delta\theta_J M_J/(J_2 M_S)$, where F_J is another constant of order unity. Again, to produce

the observed corrugation, $\delta\theta_J M_J$ would need to be of order $10^{-8} M_S$. Thus in both cases only a relatively small part of the planet needs to shift to produce the required change in Saturn's gravity field. Furthermore, the large storms that appear occasionally at Saturn [28] could be the surface manifestations of massive upflow of material. Recent observations even indicate that the overall flow of Titan's atmosphere is misaligned from the rotation axis of the solid satellite [29]. Sufficiently large changes in Saturn's internal structure therefore may have occurred in the last 30 years.

The major difficulty with the above scenarios is that these changes in the planet's internal structure alter Saturn's moments of inertia, but being internal to the planet, cannot affect Saturn's total angular momentum. For a solid body, such a misalignment between the principal inertial axes and the angular momentum always causes the body to wobble [30]. For a fluid planet, the situation is a bit more complicated because initially different parts of the planet could potentially circulate about different axes. Even so, there are only an extremely limited number of ways that the mass and angular velocity distribution within the planet can be redistributed that would keep the planet's moment of inertia aligned with the angular momentum vector. These sorts of finely tuned scenarios (for example, where the equatorial jet tilts in one direction and the rest of the planet tilts in the opposite direction to compensate) appear rather implausible at present. If the planet does wobble, then the body axes, and hence the gravitational equator plane, do not retain a fixed orientation in inertial space, but instead regress at a rate $\omega_w \sim \omega_S$ [30] about the angular momentum vector. Since the wobble frequency is not much slower than the ring's nodal regression rate, the ring particles' orbits would not maintain a fixed inclination relative to the new equator plane. Instead, the ring particles would move within a gravitational potential that on average has the same equator plane as it did before the shift, but now includes a vertical component that varies with time at the rate ω_w. This time-variable part of the potential could drive changes in ring particles' inclinations and node positions like those found at vertical resonances with inclined moons, but those effects will only be significant at specific locations in the rings where the epicyclic frequencies resonate with ω_w. These perturbations could therefore potentially drive bending waves through the rings, but would not furnish the extensive inclined sheet that we appear to have had in the D and C rings.

In conclusion, while we cannot yet rule out the possibility that a tilt in Saturn's equator plane was responsible for producing the corrugation in the C ring, we also cannot provide a plausible scenario that would be consistent with the observed data. Thus at this point we must regard shifts in Saturn's gravitational field as unlikely explanations for the C-ring corrugation, at least until a model can be developed where changes in Saturn's internal structure do not lead to a wobbling planet, or a suddenly wobbling gravitational field produces a simple inclined ring.

Supporting Text 7: Calculation of D_F for homogeneous debris clouds

As discussed in the main text, the angular momentum imparted to the rings by a debris cloud with mass m_c crossing the rings at a speed v_c can be expressed as:

$$L_c = D_F \tau m_c v_c r, \tag{S26}$$

where r is the orbital radius in the rings, τ is the normal optical depth of the rings, and D_F is a numerical factor that depends on the structure, speed and geometry of the incoming cloud. While there are no direct observations of the debris cloud that we propose struck Saturn's rings in 1983, estimates of the likely range of values for D_F can be obtained by considering idealized, spatially homogeneous debris clouds composed of particles that are all much smaller than the typical ring particle.

Assuming a spatially homogeneous cloud means that far from the planet the cloud has a constant mass volume density ρ_∞ and all the particles in the cloud are traveling at the same velocity $\mathbf{v}_\infty$ relative to Saturn. These assumptions not only simplify the calculation of D_F, but are also conservative because substructure in the cloud should increase the variations in the amount of material striking different ring longitudes and thus produce a larger net tilt in the rings.

In order to further simplify the calculations, we also assume the storm particles are sufficiently small compared to the ring particles that none of the debris from the collisions can escape the Saturn system or avoid re-impact with the rings. If this condition is met, then any debris from a collision within a moderate optical depth ring like the C ring will be swept up onto the ring particles on time scales much shorter than the relevant relative precession periods, and the ring will absorb all the incoming momenta of all the storm particles that strike ring material. (Collisions among the ring particles should also ensure that the incoming momentum from the debris particles is equitably distributed among the relevant ring particles.) While there is no direct evidence that this constraint was satisfied during in the 1983 event, it is a reasonable assumption to make given that typical C-ring particles are centimeters to meters in size [10], much larger than most of the visible dust surrounding comets.

Finally, in order to avoid complications and inefficiencies associated with changes in the ring particle's orbital parameters during the ring-tilting event, we will assume here the ring is exposed to a debris cloud for a total time t that is much less than the precession period of the rings (roughly 15 days in the C ring).

Figure S4 illustrates the geometry of this problem. All the particles in the debris cloud are

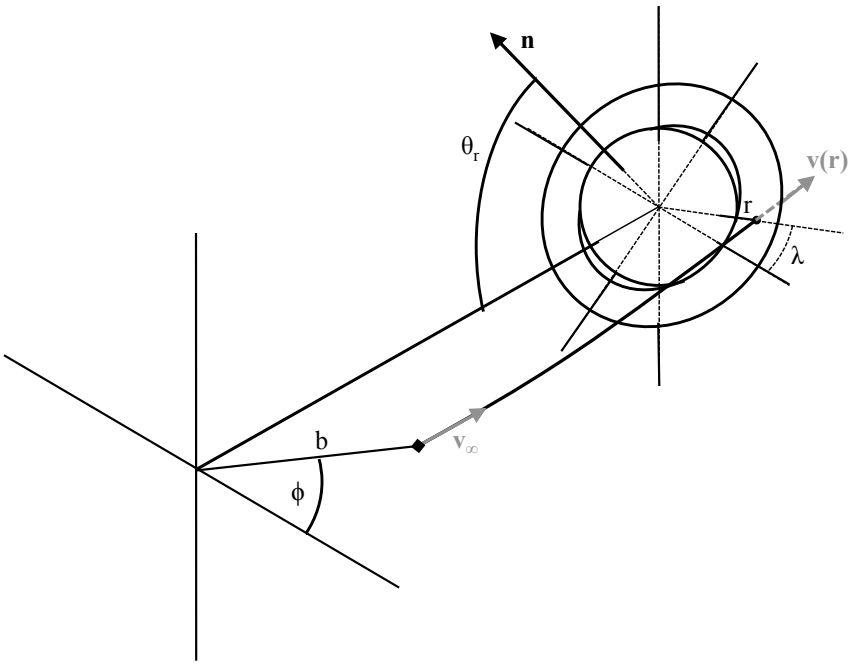

Figure S4: Geometry of the debris cloud approaching Saturn and its ring

assumed to approach Saturn from a great distance in the same direction and at the same velocity $\mathbf{v}_\infty$, but with a range of different impact parameters b and azimuth angles ϕ. The spin axis of the planet, or equivalently the surface normal of Saturn's rings $\hat{\mathbf{n}}$, is assumed to be tilted by an angle θ_r relative to the incident flow (i.e., $\theta_r = 0$ corresponds to face-on flow into the rings, and $\theta_r = \pi/2$ corresponds to edge-on flow). The coordinates of any given point in the rings are specified by a radius r and longitude λ. Both λ and ϕ are measured from an axis that is given by the cross product $\hat{\mathbf{n}} \times \mathbf{v}_\infty$.

While the ring is exposed to the debris cloud, a mass flux f_m passes through the rings. In fact, due to gravitational focusing, debris particles can in principle curve 180° around the planet to strike both faces of the rings, so there are actually two mass fluxes across the rings. We will here designate these fluxes $f_m^\pm$, where f_m^+ corresponds to particles that hit the side of the rings that faces the incident flow far from the planet (what would be the lit side of the rings if the flow were anti-aligned with the Sun), and f_m^- corresponds to the particles that strike the ring from the opposite ("unlit") face. Thus the total mass flux through the ring is the sum of these fluxes $f_m^+ + f_m^-$.

Each of the two mass fluxes will apply forces on the small patch of ring. In the continuum limit, the normal component of the force applied to a small area dA of the ring at a specified radius and longitude is given by the stress:

$$\frac{dF_n^\pm}{dA} = (1 - T^\pm) f_m^\pm (\mathbf{v}^\pm \cdot \hat{\mathbf{n}}), \tag{S27}$$

where $T^\pm$ is the transmission through the ring (i.e., the fraction of storm particles that pass through the ring without hitting any ring particles), $f_m^\pm$ is the mass flux through the ring, $\mathbf{v}^\pm$ is the velocity of the storm particles at the ring, and $\hat{\mathbf{n}}$ is the ring surface normal. Note that the transmission factor can be written in terms of the ring's normal optical depth τ:

$$1 - T^\pm = 1 - e^{-\tau/|\hat{\mathbf{v}}^\pm \cdot \hat{\mathbf{n}}|}, \tag{S28}$$

where $\hat{\mathbf{v}}^\pm$ is a unit vector aligned with the flow into the rings. For the C ring, which has a relatively low $\tau \sim 0.1$, we can approximate:

$$1 - T^\pm \simeq \frac{\tau}{|\hat{\mathbf{v}}^\pm \cdot \hat{\mathbf{n}}|}. \tag{S29}$$

So we can simplify the expression for the stress as:

$$\frac{dF_n^\pm}{dA} = \pm \tau v^\pm f_m^\pm, \tag{S30}$$

where $v^{\pm}$ is simply the speed of the storm particles as they pass through the ring. This approximation will certainly break down if the impacting flux hits the rings at such a shallow angle that $\tau/|\hat{\mathbf{v}} \cdot \hat{\mathbf{n}}|$ is not small. However we will ignore such complications here. If we assume that the storm particles all have the same speed far from the planet, then according to energy conservation the speed of the debris approaching the ring from both sides is equal, so we can set $v^+ = v^- = v_c$ and compute the net stress on the rings as:

$$\frac{dF_N}{dA} = \tau v_c (f_m^+ - f_m^-). \tag{S31}$$

In general, the mass fluxes into the rings will vary with longitude λ, so as any given patch of ring material orbits the planet, it will be exposed to varying fluxes and experience varying torques. In order for these torques to cause a tilt in the rings, the average torque density over all ring longitudes λ needs to be non-zero about some axis in the rings (i.e. it must have a component lying in the ring plane). By symmetry, we expect the stress to be an odd function of λ. Thus the net torque should have the form:

$$\frac{d\bar{\mathcal{T}}}{dA} = \tau v_c r \frac{1}{2\pi} \int (f_m^+ - f_m^-) \sin\lambda d\lambda, \tag{S32}$$

and, assuming the ring is exposed to the debris for a time t, the total angular momentum imparted to the rings per unit area is

$$\frac{dL_c}{dA} = t\frac{d\bar{\mathcal{T}}}{dA} = \tau v_c r t \frac{1}{2\pi} \int (f_m^+ - f_m^-) \sin\lambda d\lambda. \tag{S33}$$

If this is nonzero, the ring will become tilted along the axis that lies in the plane containing the incident flow vector $\mathbf{v}_\infty$ and the initial surface normal $\hat{\mathbf{n}}$.

We can also compute the average mass flux passing through the rings:

$$\bar{f} = \frac{1}{2\pi} \int (f_m^+ + f_m^-) d\lambda. \tag{S34}$$

During a time t, the total mass passing through this patch of rings can therefore be written as:

$$\frac{dm_c}{dA} = \frac{t}{2\pi} \int (f_m^+ + f_m^-) d\lambda. \tag{S35}$$

Combining Eqs. S33 and S35, we can obtain an expression analogous to Eq. S26:

$$\frac{dL_c}{dA} = D_F \tau \frac{dm_c}{dA} v_c r, \tag{S36}$$

where

$$D_F = \frac{\int (f_m^+ - f_m^-) \sin\lambda d\lambda}{\int (f_m^+ + f_m^-) d\lambda} \tag{S37}$$

is an explicit expression for D_F in terms of the integrated mass fluxes.

To evaluate the above expression for D_F, we need to consider in more detail the trajectories of the storm particles into the rings. Given the approximate spherical symmetry of the gravity field, it is easiest to describe the storm-particle's trajectories in terms of Saturn-centered spherical polar coordinates r, θ (polar angle) and ϕ (azimuth angle). It is also simplest to align this coordinate system such that the debris particles all approach the planet from $\theta \simeq 0$, then for any given particle's trajectory, ϕ will remain constant and any trajectory can be expressed as $r(\theta)$. Note that along a particles' trajectory, θ may sweep more than 180° as the particle swings around the planet, so we must allow θ to range from 0 to 2π along the particle's trajectory. Assuming the surface normal of the rings $\hat{\mathbf{n}}$ is tilted by an angle θ_r relative to the incident flow direction (see Figure S4) then the θ, ϕ coordinates of a ring patch at longitude λ is given by :

$$\cos\theta = -\sin\lambda \sin\theta_r \tag{S38}$$

$$\tan\phi = \tan\lambda \cos\theta_r. \tag{S39}$$

The latter allows $\sin\lambda$ to be written as a function of ϕ:

$$\sin\lambda = \frac{\sin\phi}{\sqrt{\sin^2\phi \sin^2\theta_r + \cos^2\theta_r}}. \tag{S40}$$

Combined with Eq. S38 above, the polar angle θ at the ring can be expressed as a function of ϕ

$$\cos\theta = \frac{-\sin\phi \sin\theta_r}{\sqrt{\sin^2\phi \sin^2\theta_r + \cos^2\theta_r}} \tag{S41}$$

$$\sin\theta = \frac{\cos\theta_r}{\sqrt{\sin^2\phi \sin^2\theta_r + \cos^2\theta_r}}. \tag{S42}$$

A particle crossing the ring at a given r and λ can also be tracked back to a starting point far from the planet with impact parameter b and azimuth ϕ. A patch of the ring between radii of r and $r + dr$ and longitudes of λ and $\lambda + d\lambda$ therefore maps to a region of the incident flow between impact parameters of b and $b + db$, and azimuths between ϕ and $\phi + d\phi$. In the steady state, the total mass of debris passing through the ring patch in a given time must equal the integrated flux

over the corresponding area in the incident flow. This means:

$$f_m^{\pm} r dr d\lambda = f_{m,\infty} b^{\pm} db^{\pm} d\phi, \tag{S43}$$

where $f_{m,\infty}$ is the incident mass flux far from Saturn, which is simply $\rho_\infty v_\infty$, so we can express the flux into the rings as:

$$f_m^{\pm} = \rho_\infty v_\infty \frac{b^{\pm}}{r} \frac{db}{dr}^{\pm} \frac{d\phi}{d\lambda}. \tag{S44}$$

This function, however, assumes that the particles are actually able to reach the ring. In practice, the planet will block particles from reaching some parts of the ring. We can account for this possibility by defining "blocking functions" $K^{\pm}$. These functions equal zero if the storm particles are blocked from reaching a given point on the rings and are one otherwise. Thus the fluxes are actually:

$$f_m^{\pm} = \rho_\infty v_\infty K^{\pm} \frac{b^{\pm}}{r} \frac{db}{dr}^{\pm} \frac{d\phi}{d\lambda}. \tag{S45}$$

Inserting these expressions into Eq. S37, we find

$$D_F = \frac{\int \left(K^+ \frac{b^+}{r} \frac{db}{dr}^+ - K^- \frac{b^-}{r} \frac{db}{dr}^- \right) \frac{\sin\phi d\phi}{\sqrt{\sin^2\phi \sin^2\theta_r + \cos^2\theta_r}}}{\int \left(K^+ \frac{b^+}{r} \frac{db}{dr}^+ + K^- \frac{b^-}{r} \frac{db}{dr}^- \right) d\phi}. \tag{S46}$$

Note that the leading factors of ρ_∞ and v_∞ drop out, as one should expect since D_F is a unitless quantity in Eqs. S26 and S36.

In order to make further progress, we need to evaluate expressions for b and db/dr as functions of r and θ. Thus let us consider the trajectory of a single particle in the storm. Since the particles far from Saturn have a finite speed v_∞, these particles all follow hyperbolic trajectories of the form:

$$r = \frac{p(1+e)}{1 + e\cos(\theta - \theta_p)}, \tag{S47}$$

where p and $e > 1$ are the pericenter distance and the eccentricity of the hyperbolic orbit, and θ_p determines the location of the orbit's periapse. Recall we are assuming that the storm particles all approach the planet from the $+z$ direction, so r must approach infinity as θ approaches 0. This requires that $\cos\theta_p = -1/e$, so we can re-write the above equation as:

$$r = \frac{p(1+e)}{1 - \cos\theta + \sqrt{e^2-1}\sin\theta}. \tag{S48}$$

We can now express the parameters p and e in terms of v_∞ and b. Conservation of energy and

angular momentum between infinity and pericenter requires that:

$$v_\infty b = v_p p \tag{S49}$$

and

$$v_\infty^2 = v_p^2 - \frac{2GM}{p}, \tag{S50}$$

where v_p is the velocity of the particle at periapse. Combining these two expressions to eliminate v_p, we obtain the following expression for p:

$$p = b\left[\sqrt{\left(\frac{GM}{v_\infty^2 b}\right)^2 + 1} - \frac{GM}{v_\infty^2 b}\right]. \tag{S51}$$

We can determine e using the standard expression for v_∞:

$$v_\infty = \sqrt{\frac{GM}{-a}}, \tag{S52}$$

where $-a = p/(e-1)$ is the orbit's semi-major axis. Solving for e and inserting the above expression for p, we get:

$$e = \sqrt{\left(\frac{v_\infty^2 b}{GM}\right)^2 + 1}. \tag{S53}$$

Inserting these two expressions into Eq. S48, we find:

$$r = \frac{v_\infty^2 b^2}{GM}\left[1 - \cos\theta + \frac{v_\infty^2 b}{GM}\sin\theta\right]^{-1}. \tag{S54}$$

Solving this expression for b, we can find the original impact parameter of a storm particle that hits the ring at a given radius r and angle θ:

$$b = \frac{r}{2}\left[\sqrt{\sin^2\theta + \frac{4GM}{v_\infty^2 r}(1-\cos\theta)} + \sin\theta\right] \tag{S55}$$

and taking the derivative of this expression, we find:

$$\frac{db}{dr} = \frac{\frac{GM}{v_\infty^2 r}(1-\cos\theta) + \frac{1}{2}\sin^2\theta + \frac{1}{2}\sin\theta\sqrt{\sin^2\theta + \frac{4GM}{v_\infty^2 r}(1-\cos\theta)}}{\sqrt{\sin^2\theta + \frac{4GM}{v_\infty^2 r}(1-\cos\theta)}}. \tag{S56}$$

Recalling the definition of circular orbital velocity $v_o = \sqrt{GM/r}$, we can re-write these expressions

as:

$$\frac{b^+}{r} = \frac{1}{2}\left[\sqrt{\sin^2\theta + \frac{4v_o^2}{v_\infty^2}(1-\cos\theta)} + \sin\theta\right] \tag{S57}$$

and

$$\frac{db^+}{dr} = \frac{\frac{v_o^2}{v_\infty^2}(1-\cos\theta) + \frac{1}{2}\sin^2\theta + \frac{1}{2}\sin\theta\sqrt{\sin^2\theta + \frac{4v_o^2}{v_\infty^2}(1-\cos\theta)}}{\sqrt{\sin^2\theta + \frac{4v_o^2}{v_\infty^2}(1-\cos\theta)}}. \tag{S58}$$

Note that we have now explicitly identified these factors as applying to the particles that strike the side of the ring facing the incoming debris cloud. For these functions, θ lies in the range between 0 and π. However, there is nothing to prevent the particles from following trajectories beyond $\theta = \pi$ as they pass close to Saturn, so we can continue the trajectories around Saturn's far side and determine the factors appropriate for the storm particles striking the back side of the ring by replacing θ with $2\pi - \theta$ in the above expressions. This means $\cos\theta \to \cos\theta$ and $\sin\theta \to -\sin\theta$, so the resulting expressions for b^- and db^-/dr are

$$\frac{b^-}{r} = \frac{1}{2}\left[\sqrt{\sin^2\theta + \frac{4v_o^2}{v_\infty^2}(1-\cos\theta)} - \sin\theta\right] \tag{S59}$$

and

$$\frac{db^-}{dr} = \frac{\frac{v_o^2}{v_\infty^2}(1-\cos\theta) + \frac{1}{2}\sin^2\theta - \frac{1}{2}\sin\theta\sqrt{\sin^2\theta + \frac{4v_o^2}{v_\infty^2}(1-\cos\theta)}}{\sqrt{\sin^2\theta + \frac{4v_o^2}{v_\infty^2}(1-\cos\theta)}}. \tag{S60}$$

Now we need to determine the how blocking functions $K^\pm$ vary with r and θ. Obviously, for a storm particle to be blocked by the planet, the periapse distance p must be less than the planet's radius R_s. From Eq. S51 we can derive an expression for b as a function of p:

$$b = p\sqrt{1 + \frac{2GM}{v_\infty^2 p}} \tag{S61}$$

Thus the critical impact parameter:

$$b_c = R_s\sqrt{1 + \frac{2GM}{v_\infty^2 R_s}} \tag{S62}$$

such that, if $b < b_c$, then the particles will impact the planet, and if $b > b_c$, then the particles will miss the planet.

However just because the particles eventually impact the planet does not mean they could not hit the rings first. Particles with $b < b_c$ will still be able to reach the rings if they encounter the

rings at an angle $\theta < \theta_p$. Note that θ_p must be between $\pi/2$ and π. Thus a particle with $b < b_c$ will always impact the planet before it can reach the back face of the rings. By contrast, particles approaching the front face of the rings will only be blocked when $\theta > \theta_p$, or, equivalently (using Eq. S53) when:

$$\cos\theta < \cos\theta_p = -\frac{1}{e} = -\left[\left(\frac{v_\infty^2 b}{GM}\right)^2 + 1\right]^{-1/2}. \tag{S63}$$

Thus the blocking functions are:

$$K^+ = \Theta(b^+ - b_c) + \Theta(b_c - b^+)\Theta(\cos\theta - \cos\theta_p) \tag{S64}$$

and

$$K^- = \Theta(b^- - b_c), \tag{S65}$$

where $\Theta(x)$ are Heaviside step functions for argument x.

Inserting the above expressions for $b^\pm/r$, $db^\pm/dr$ and $K^\pm$ into Eq. S46 for D_F clearly yields rather complex expressions. However, these integrals can be evaluated numerically to yield Fig. S5, which shows D_F as a function of tilt angle for several different values of v_∞ and a single radius in the rings. These curves have unusual shapes that arise because two different mechanisms can generate the asymmetries in the integrated flux needed to produce the observed tilt. On the one hand, the planet can simply block debris from reaching certain longitudes. On the other hand, gravitational focusing by the planet can deliver more material to certain longitudes than others. The competition between these two mechanisms leads to the complex shapes of these curves. Nevertheless, it is clear that for a broad range of conditions, D_F is of order 10%.

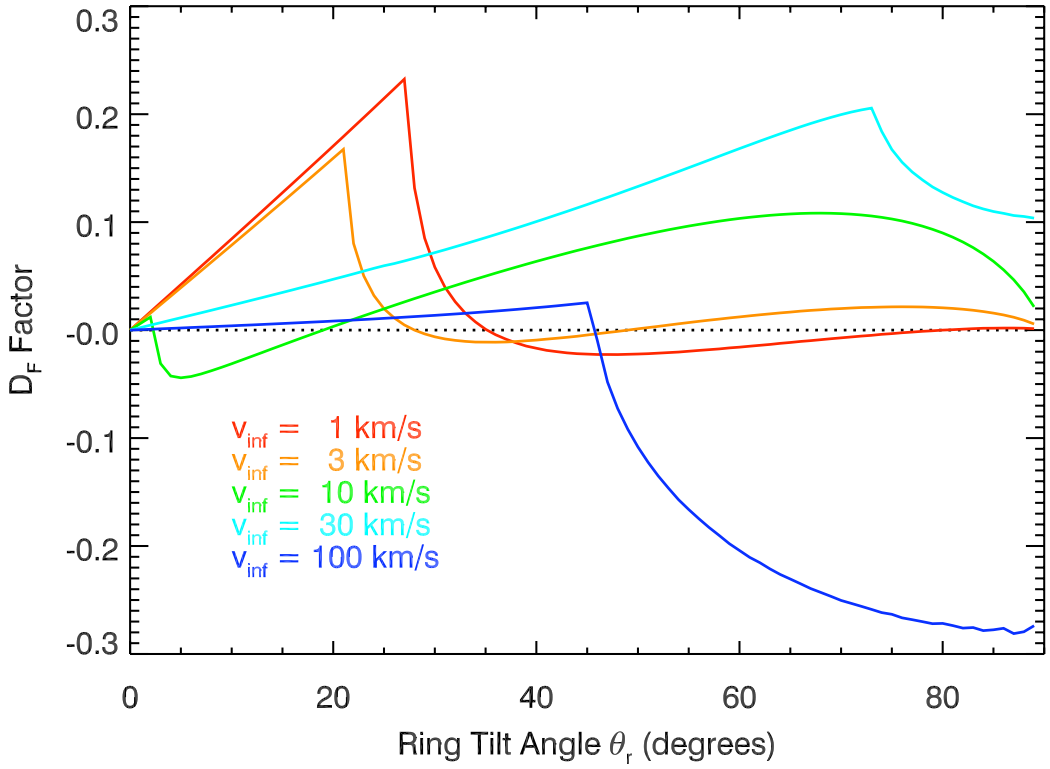

Figure S5: Plot of the factor D_F at a radius of $80,000$ km in Saturn's rings as a function of the ring tilt angle θ_r for several different values of v_∞.

Supporting Text 8: Break-up of Comets in the Saturn System

As alternatives to the scenario described in the main text, we have considered the possibility that a comet was catastrophically disrupted during its passage through the Saturn system, and the debris from that event rained down on the ring before it could again escape into interplanetary space. Three processes may disrupt a comet in the Saturn system: (1) tidal stresses during a close pass by the planet, (2) high-velocity collisions with objects in orbit around Saturn, and (3) excessive ram pressures in the upper layers of Saturn's atmosphere.

In practice, the first two options seem unlikely because in both these cases it is difficult to deliver the debris appropriately into the C ring along purely ballistic trajectories. Tidal disruption tends to disperse material almost entirely along the original projectile's orbit track [11]. Hence, unless some other process further disperses the material, all the resulting debris would pass through the rings at approximately the same radius and longitude, and not rain down across the entire region now covered by the corrugation (dispersion by solar radiation pressure, like that proposed for the debris striking Jupiter's rings [3], will not be effective on the short time scales of a single periapse passage). On, the other hand, the only place in the Saturn system that the comet is likely encounter an object that would cause it to shatter is within the main rings. However, no hyperbolic trajectory exists that can intersect the rings twice –once between 75,000 and 92,000 km– while missing the planet (at 60,300 km) in between. Thus the debris from the first ring passage cannot reach the C ring to produce the corrugation.

With the first two options eliminated as viable scenarios, the only remaining possibility is that the comet broke apart as it passed through the upper layers of Saturn's atmosphere. In this scenario, the debris must pass sufficiently deeply through the atmosphere to be disrupted but not so deep that it cannot again emerge from the atmosphere. The atmosphere will cause the object to fragment when the ram pressure exceeds the material strength of the object [31, 32]. Estimates of the tensile strength of comet nuclei generally lie in the range of $\sim 10^2 - 10^4$ N/m^2 [33], while the ram pressure on an object moving through an atmosphere is given by the expression: $P_{ram} = n_a m_a v^2$ where n_a is the local atmospheric number density, m_a is the average molecular mass, and v is the velocity of the object through the atmosphere. Assuming $m_a \sim 2$ amu and $v \sim 40$ km/s, we can estimate that a comet will fragment in Saturn's atmosphere when the number density exceeds $10^{13} - 10^{15}$/cm^3. Such number densities are found between 500 and 1000 km above the 1-bar level [34].

In order to reach the outer parts of the C ring, the debris must leave the atmosphere with a speed of ~ 30 km/s. The deceleration of a piece of debris of radius r_d, mass m_d and mass density

$\rho_d \sim 1000$ kg/m^3 within the atmosphere can be derived from the ram pressure [35, 32]:

$$\frac{dv}{dt} = -\frac{P_{ram}}{m_d}\pi r_d^2 = -\frac{3m_a v^2}{4\rho r_d} n_a. \tag{S66}$$

Integrating this expression over the entire track through the atmosphere (which we may approximate as straight), we find the final velocity of the debris is:

$$v_f = v_i e^{-3m_a N_a/4\rho r_d}, \tag{S67}$$

where v_i is the initial velocity of the debris and N_a is the total column density of molecules along the path. If we assume $v_i \sim 40$ km/s, then in order for v_f to exceed 30 km/s, N_a needs to be less than $\sim 10^{19}$/cm$^2 * (r_d/1\mu$m). The column density N_a will only exceed 10^{19}/cm^2 when the path reaches deeper than ∼300 km above the 1-bar level [34], so there is a few-hundred kilometer wide region where a comet could break up and even micron-sized grains could potentially escape from the planet and make it to the outer C ring. Furthermore, if the debris consists of particles with a range of sizes, they will emerge from the planet with a range of velocities, which will help disperse the material before it encounters the rings.

The rate of such Saturn-grazing impacts can be estimated from the present-day flux of the required ∼1 km-sized objects in the outer solar system. Numerical simulations show that the impact flux into Saturn is ∼0.4 times the impact flux into Jupiter [16, 17]. As discussed in the main text, the observation of a fresh impact scar on Jupiter in 2009 [37] may imply that the impact rate of roughly 1-km-sized objects into Jupiter could be as high as 10 per century [21]. If this higher rate is correct, then we expect roughly four such objects would strike Saturn every century. Of course, the impactor needs to have a rather specific trajectory in order to both skim through the atmosphere and then collide with the rings. The few-hundred-kilometer-wide shell in Saturn's atmosphere the comet needs to pass through has about 1% the cross sectional area of the entire planet, and only about 10% of the quasi-linear trajectories passing through this region would then pass through the C ring. The rate of Saturn-grazing C-ring impactors should therefore be about 10^3 times lower than the impact rate into Saturn. If we expect four 1-km-wide comets to collide with Saturn per century then a collision with a geometry that could yield the desired ring-impacting debris cloud would only occur about every 25,000 years. This mechanism therefore generates suitable debris clouds less frequently than the temporarily captured objects described in the main text, and there is only a ∼0.1% chance that such an event has occurred in the last 30 years.

References and Notes

[1] M. M. Hedman, *et al.*, Saturn's dynamic D ring. *Icarus* **188**, 89-107 (2007).

[2] M. E. Ockert-Bell, *et al.*, The Structure of Jupiter's Ring System as Revealed by the Galileo Imaging Experiment. *Icarus* **138**, 188-213 (1999).

[3] M. R. Showalter, M. M. Hedman, J.A. Burns, The impact of comet Shoemaker-Levy 9 sends ripples through the rings of Jupiter. *Science* this issue (2011).

[4] C. D. Murray, S. F. Dermott, *Solar System Dynamics* (Cambridge University Press, 1999).

[5] For Saturn's C ring, higher-order gravity harmonics, mainly J_4 [6] only contribute a total of <10% to the nodal regression rate and 10-15% to the gradient of the nodal regression rate.

[6] R. A. Jacobson, *et al.*, The gravity field of the Saturnian system from satellite observations and spacecraft tracking data. *AJ* **132**, 2520-2526 (2006).

[7] H. A. Zebker, E. A. Marouf, G. L. Tyler, Saturn's rings - Particle size distributions for thin layer model. *Icarus* **64**, 531-548 (1985).

[8] P. A. Rosen, G. L. Tyler, E. A. Marouf, J. J. Lissauer, Resonance structures in Saturn's rings probed by radio occultation. II - Results and interpretation. *Icarus* **93**, 25-44 (1991).

[9] The error estimate includes ±10 days of statistical error, ±13 days uncertainty from the published estimate of J_6 [6], ±13 days from allowing J_8 to range between 0 and -0.00001, and ±5 days that depends on whether the wavenumbers are corrected for the ring's predicted mass. Additional uncertainty could be introduced if J_{10} and higher-order terms in Saturn's gravity field are sufficiently large.

[10] J. N. Cuzzi, *et al.*, *Saturn From Cassini-Huygens*, M.K. Dougherty, L.W. Esposito, & S.M. Krimigis, ed. (Springer, 2009), pp. 459-509.

[11] J. V. Scotti, H. J. Melosh, Estimate of the size of comet Shoemaker-Levy 9 from a tidal breakup model. *Nature* **365**, 733-735 (1993).

[12] E. Asphaug, W. Benz, Size, Density, and Structure of Comet Shoemaker-Levy 9 Inferred from the Physics of Tidal Breakup. *Icarus* **121**, 225-248 (1996).

[13] M. Montalto, A. Riffeser, U. Hopp, S. Wilke, G. Carraro, The comet 17P/Holmes 2007 outburst: the early motion of the outburst material. *A&A* **479**, L45-L49 (2008).

[14] Scenarios in which the debris from the disrupted comet hits the rings before it can leave the inner Saturn system are explored in SOM text 8 and are found to be less probable.

[15] D. M. Kary, L. Dones, Capture statistics of short-period comets: Implications for comet D/Shoemaker-Levy 9. *Icarus* **121**, 207-224 (1996).

[16] H. F. Levison, M. J. Duncan, From the Kuiper Belt to Jupiter-Family Comets: The spatial distribution of ecliptic comets. *Icarus* **127**, 13-32 (1997).

[17] K. Zahnle, P. Schenk, H. Levison, L. Dones, Cratering rates in the outer Solar System. *Icarus* **163**, 263-289 (2003).

[18] H. F. Levison, M. J. Duncan, K. Zahnle, M. Holman, L. Dones, NOTE: Planetary impact rates from ecliptic comets. *Icarus* **143**, 415-420 (2000).

[19] S. Charnoz, A. Morbidelli, L. Dones, J. Salmon, , Did Saturn's rings form during the Late Heavy Bombardment? *Icarus* **199**, 413-428 (2009).

[20] This rate may be conservative because none of the referenced simulations include Saturn's rings, which could not only disrupt incoming comets but also withdraw some momentum from the debris, increasing its chances of being captured into orbit around Saturn.

[21] A. Sánchez-Lavega, *et al.*, The impact of a large object on Jupiter in 2009 July. *ApJL* **715**, L155-L159 (2010).

[22] C. C. Porco, *et al.*, Cassini imaging science: Instrument characteristics and anticipated scientific investigations at Saturn. *Space Science Reviews* **115**, 363-497 (2004).

[23] S. Chandrasekhar, *Radiative Transfer* (Dover, 1960).

[24] F. H. Shu, *Planetary Rings*, R. Greenberg, A. Brahic, eds. (1984), pp. 513–561.

[25] J. E. Colwell, J. H. Cooney, L. W. Esposito, M. Sremčević, Density waves in Cassini UVIS stellar occultations. 1. The Cassini Division. *Icarus* **200**, 574-580 (2009).

[26] P. A. Rosen, J. J. Lissauer, The Titan-1:0 nodal bending wave in Saturn's Ring C. *Science* **241**, 690-694 (1988).

[27] P. A. Rosen, G. L. Tyler, E. A. Marouf, Resonance structures in Saturn's rings probed by radio occultation. I - Methods and examples. *Icarus* **93**, 3-24 (1991).

[28] A. Sanchez-Lavega, *et al.*, The Great White Spot and disturbances in Saturn's equatorial atmosphere during 1990. *Nature* **353**, 397-401 (1991).

[29] R. K. Achterberg, B. J. Conrath, P. J. Gierasch, F. M. Flasar, C. A. Nixon, Observation of a tilt of Titan's middle-atmospheric superrotation. *Icarus* **197**, 549-555 (2008).

[30] R. Baierlein, *Newtonian Dynamics* (McGraw-Hill, 1983).

[31] C. F. Chyba, P. J. Thomas, K. J. Zahnle, The 1908 Tunguska explosion - Atmospheric disruption of a stony asteroid. *Nature* **361**, 40 (1993).

[32] J. G. Hills, M. P. Goda, The fragmentation of small asteroids in the atmosphere. *AJ* **105**, 1114-1144 (1993).

[33] J. Rahe, V. Vanysek, P. R. Weissman, *Hazards Due to Comets and Asteroids*, T. Gehrels, M. S. Matthews, & A. M. Schumann, ed. (1994), pp. 597-634.

[34] A. F. Nagy, *et al.*, *Saturn From Cassini-Huygens*, M.K. Dougherty, L.W. Esposito, & S.M. Krimigis, ed. (Springer, 2009), pp. 181–201.

[35] J. B. Pollack, J. A. Burns, M. E. Tauber, Gas drag in primordial circumplanetary envelopes - A mechanism for satellite capture. *Icarus* **37**, 587-611 (1979).

[36] J. H. Rogers, The comet collision with Jupiter: II. The visible scars. *Journal of the British Astronomical Association* **106**, 125-149 (1996).

[37] A. Wesley, Impact mark discovered on Jupiter by Australian amateur astronomer. Presented at European Planetary Science Congress 2009, Potsdam Germany, held 14-18 September 2009.

Acknowledgments: We acknowledge the support of the ISS team and the Cassini Project, as well as NASA's Planetary Geology and Geophysics and Cassini Data Analysis programs. We also wish to thank M.R. Showalter, P.D. Nicholson, S. Charnoz, L. Dones and D.P. Hamilton for useful conversations.